DMT1 Inhibitors Kill Cancer Stem Cells by Blocking Lysosomal Iron Translocation

Andreea Turcu, Antoine Versini, Nadjib Khene, Christine Gaillet, Tatiana Cañeque, Sebastian Müller, Raphaël Rodriguez

CHEMISTRY
A European Journal

A Journal of
ChemPubSoc Europe

Accepted Article

Title: DMT1 Inhibitors Kill Cancer Stem Cells by Blocking Lysosomal Iron Translocation

Authors: Andreea L. Turcu, Antoine Versini, Nadjib Khene, Christine Gaillet, Tatiana Cañeque, Sebastian Müller, and Raphaël Rodriguez

To be cited as: *Chem. Eur. J.* 10.1002/chem.202000159

Link to VoR: http://dx.doi.org/10.1002/chem.202000159

Supported by
ACES

WILEY-VCH

10.1002/chem.202000159

DMT1 Inhibitors Kill Cancer Stem Cells by Blocking Lysosomal Iron Translocation

Andreea L. Turcu,[1†] Antoine Versini,[2,3,4†] Nadjib Khene,[2,3,4] Christine Gaillet,[2,3,4] Tatiana Cañeque,[2,3,4] Sebastian Müller,[2,3,4*] Raphaël Rodriguez[2,3,4*]

[1]Laboratori de Química Farmacèutica (Unitat Associada al CSIC), Facultat de Farmàcia i Ciències de l'Alimentació i Institut de Biomedicina, University of Barcelona, Av. Joan XXIII, 27-31, 08028, Barcelona, Spain.

[2]Institut Curie, 26 rue d'Ulm, 75248 Paris Cedex 05, France.

[3]PSL Université Paris, France.

[4]Chemical Biology of Cancer Laboratory, CNRS UMR 3666, INSERM U1143.

[†] These authors contributed equally to this work.

*Correspondence to: sebastian.muller@curie.fr, raphael.rodriguez@curie.fr

Abstract

Cancer stem cells (CSC) constitute a subpopulation of cells in solid tumors that is responsible for resistance to conventional chemotherapy, metastasis and cancer relapse. The natural product Salinomycin can selectively target this cell niche by directly interacting with lysosomal iron, taking advantage of upregulated iron homeostasis in CSC. Here, we identify inhibitors of the divalent metal transporter 1 (DMT1) that selectively target CSC by blocking lysosomal iron translocation. This leads to lysosomal iron accumulation, production of reactive oxygen species and cell death with features of ferroptosis. DMT1 inhibitors selectively target CSC in primary cancer cells and circulating tumor cells, demonstrating the physiological relevance of this strategy. Taken together, this opens up opportunities to tackle unmet needs in anti-cancer therapy.

Tumors consist of heterogenous cell populations, among which a subset is responsible for metastasis formation, cancer relapse and in many cases treatment resistance, constituting a major drawback for the success of conventional anti-cancer therapy. These so-called 'cancer stem cells' (CSC) are highly plastic and can transition reversibly between epithelial and mesenchymal states[1] with distinct biochemical signatures, which opens up opportunities for therapeutic intervention[2]. Their metastable mesenchymal state is characterized by an addiction

to iron[3], providing the means to specifically target and eradicate this cancer cell population. One of the most promising small molecules that specifically targets CSC is the natural product Salinomycin[4] (**1**) (Scheme 1). It selectively kills CSC by sequestering lysosomal iron, leading to the production of reactive oxygen species (ROS) via Fenton chemistry, lysosomal membrane permeabilization and subsequent cell death reminiscent of ferroptosis[3a]. Thus, strategies to retain iron in lysosomes[3a, 5] represent an attractive therapeutic strategy to target and eradicate CSC. A key protein in the regulation of iron homeostasis is the divalent metal transporter 1 (DMT1) located within the plasma membrane and membranes of late endosomes and lysosomes, which enables the translocation of ferrous iron (Fe^{2+}) to the cytosol following iron endocytosis[6]. Thus, we hypothesized that inhibiting DMT1 could prevent iron translocation, potentially leading to lysosomal iron overload, ROS production and cell death, providing a novel therapeutic angle to eradicate iron-addicted CSC.

To this end, we synthesized a library of small molecules previously reported as DMT1 inhibitors, which can be classed into three groups: 1) ebselen (**2**)[7], 2) substituted pyrazoles (**3a**-**e**)[8] and 3) benzylisothioureas (**4a**-**e**)[9] (Scheme 1, Supplementary Information).

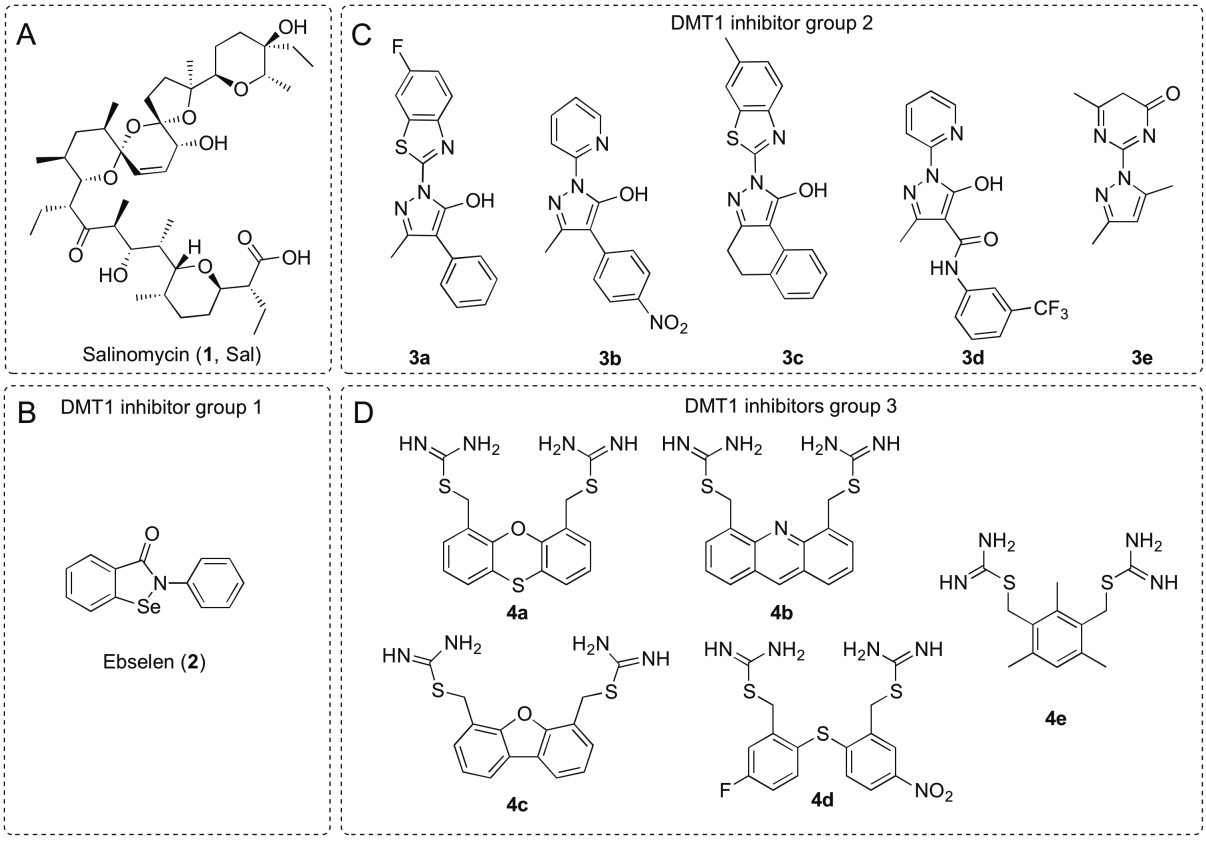

Scheme 1. Molecular structures of small molecules reported as DMT1 inhibitors. **A)** Salinomycin. **B)** Ebselen. **C)** Substituted pyrazoles. **D)** Benzylisothioureas.

Next, we evaluated the biological activity of this library of DMT1 inhibitors against transformed human mammary HMLER[10] $CD44^{high}/CD24^{low}$ cells, a well-established model of breast CSC, and their HMLER $CD44^{low}/CD24^{high}$ counterparts deprived of CSC properties, using **1** as a positive control. In this assay, a small molecule selective for CSC preferentially kills the HMLER $CD44^{high}/CD24^{low}$ cell population, as reported for **1**[3a]. We observed that DMT1 inhibitors of group 2 (**3a-e**) exhibited IC_{50} concentrations of cell viability against HMLER $CD44^{high}/CD24^{low}$ in the low micromolar range (Table 1, Figure S1). In contrast, IC_{50} values of structurally distinct molecule **2** and group 3 (**4a-e**) were more elevated. Importantly, almost all the molecules showed selectivity for HMLER $CD44^{high}/CD24^{low}$ cells exhibiting CSC properties, as defined by the ratio of IC_{50} HMLER $CD44^{low}/CD24^{high}$ (Table 1). Interestingly, while **1** exhibited a selectivity of 4.1 fold, we found that **3d** exhibited a 2.8 fold and **4a** a 2.6 fold selectivity in this model.

	IC_{50} HMLER $CD44^{low}$	IC_{50} HMLER $CD44^{high}$	Ratio HMLER $CD44^{low}/CD44^{high}$
1	5.8	1.4	**4.1**
2	19.4	18.0	**1.1**
3a	3.1	2.5	**1.2**
3b	0.4	0.3	**1.3**
3c	2.1	1.4	**1.5**
3d	1.1	0.4	**2.8**
3e	16.4	12.6	**1.3**
4a	13.9	5.4	**2.6**
4b	3.9	3.0	**1.3**
4c	16.7	10.2	**1.6**
4d	37.2	20.5	**1.8**
4e	101.3	108.8	**0.9**

Table 1. IC_{50} values of cell viability at 72 h measured for HMLER $CD44^{low}/CD24^{high}$ and HMLER $CD44^{high}/CD24^{low}$ cells in cells treated with **1** and the DMT1 inhibitors **2-4e**. Selectivity ratios ($CD44^{low}/CD44^{high}$) are indicated, with values >1 indicating a selectivity for cells with CSC properties.

These results indicated that DMT1 inhibitors show a preference for cells with features of CSC, which prompted us to investigate their mechanism of action. To this end, we used the Fe^{2+}-specific turn-on fluorescent probe RhoNox-M, which can detect the presence of Fe^{2+} in lysosomes[11], and monitored lysosomal Fe^{2+} by means of flow cytometry (Figure 1A). Whereas previous studies employed an assay using calcein quenching to assess cellular iron, using RhoNox-M allowed us to directly investigate lysosomal iron in relation to DMT1. Like **1**, compounds **3a-e** showed a pronounced increase of lysosomal Fe^{2+}. In comparison, a moderate increase of lysosomal Fe^{2+} was observed for **4a-d** but not for **4e** or **2**. The moderate

10.1002/chem.202000159

efficacy of **4e** may be assigned to a distinct configuration of the isothiourea moieties compared to **4a-d**, which may differentially affect target engagement. Although previously reported as a DMT1 inhibitor, ebselen (**2**) was also reported as a ROS scavenger preventing ferroptotic cell death[12]. Thus, reported effects on iron homeostasis might be linked to this effect as opposed to a direct inhibition of DMT1 *per se*. Thus, the lack of increased lysosomal iron loading together with the absence of selectivity for HMLER CD44^{high}/CD24^{low} cells makes **2** a suitable negative control in our settings.

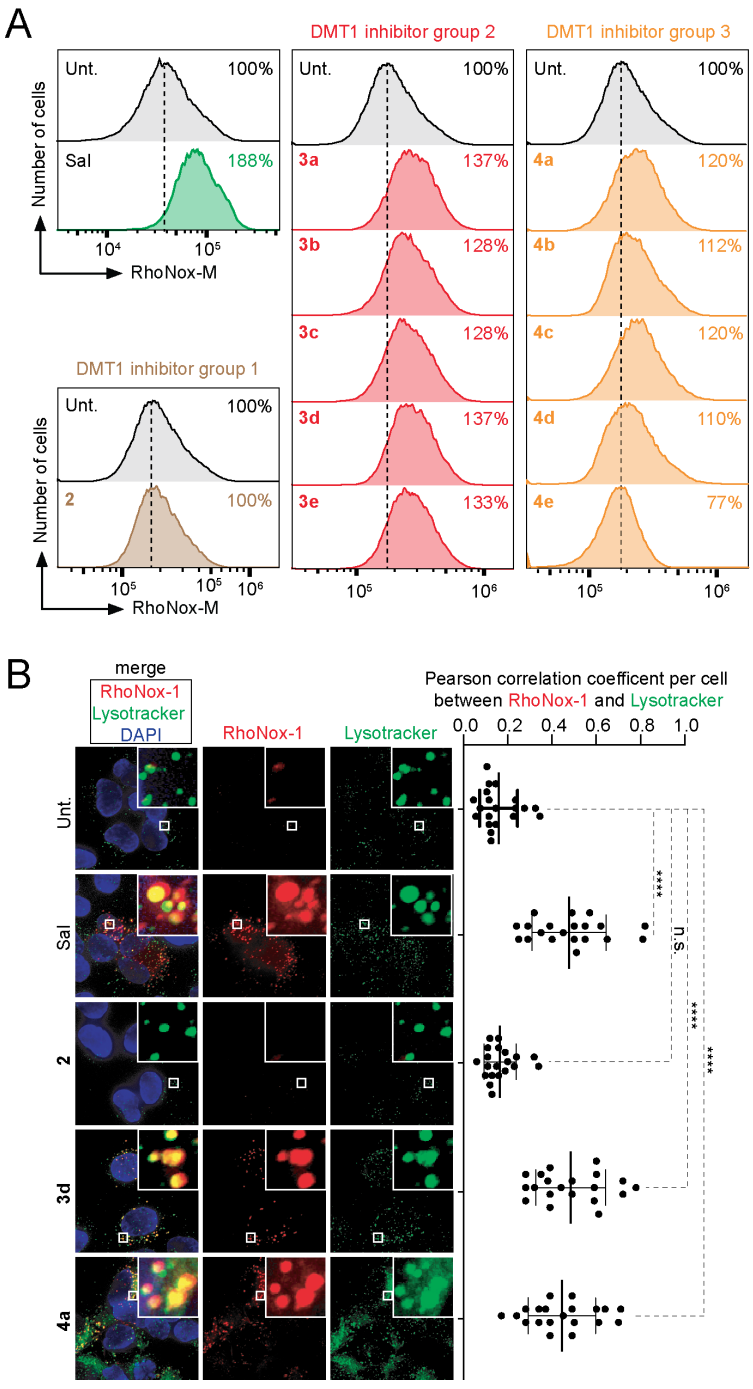

Figure 1. DMT1 inhibitors 3d and 4a increase lysosomal Fe^{2+} loading. A) Flow cytometry analysis of RhoNox-M fluorescence in cells treated with **1**, **2**, **3a-e** and **4a-e** for 24 h. **B)**

Fluorescence microscopy images of RhoNox-1 and lysotracker in cells treated with **1**, **2**, **3d** and **4a** for 24 h. Lysotracker deep red stains the lysosomes (green) and DAPI stains nuclear DNA (blue). Scale bar, 10 μm. Quantification of 20 cells per condition. $N = 3$ biological replicates. Colocalization analyses expressed as Pearson correlation coefficients. Kruskal-Wallis test with Dunn's correction. Bars and error bars, mean values +/- SD. * $P \leq 0.05$, ** $P \leq 0.01$, *** $P \leq 0.001$, **** $P \leq 0.0001$. HMLER $CD44^{high}/CD24^{low}$ cells were used throughout the figure.

To further investigate the cellular mechanisms of action (MoA), we took forward the most selective molecule of groups 2 and 3 of structurally distinct DMT1 inhibitors, namely **3d** and **4a**, using **1** and **2** as positive and negative controls, respectively. We treated cells with each molecule and monitored lysosomal iron loading using a related fluorescent Fe^{2+} selective turn-on probe RhoNox-1[13] and lysotracker. In untreated (Unt.) cells and in cells treated with **2**, we observed a weak and diffuse staining of RhoNox-1, whereas cells treated with **1**, **3d** and **4a** exhibited an increase in fluorescence, specifically localized in lysosomal compartments as defined by colocalization with lysotracker. This data indicated that these molecules block the translocation of Fe^{2+} from the lumen of lysosomes to the cytosol, thereby leading to increased lysosomal iron loading (Figure 1B).

Next, we investigated whether molecules **3d** and **4a** induced lysosomal ROS production, leading on from their lysosomal Fe^{2+} loading properties. To this end, we monitored by flow cytometry the levels of ROS using the CellROX probe, and found that **1**, **3d** and **4a** promoted the production of ROS. In contrast, levels of ROS in cells treated with compound **2** were lower and comparable to that found in untreated cells (Figure 2A). Consistent with the accumulation of iron in lysosomes, fluorescence microscopy indicated the production of ROS in this organelle in cells treated with **1**, **3d** and **4a**, as assessed by colocalization analyses of CellROX and lysotracker (Figure 2B). This, in turn, leads to lysosomal membrane permeabilization (LMP), as defined by the release of Dextran-FITC (Figure S2). In agreement with LMP, we observed increased levels of lipid ROS in cells treated with **3d** and **4a** (Figure 2C and Figure S3), suggesting a cell death mechanism sharing molecular features with ferroptosis[3a, 14].

10.1002/chem.202000159

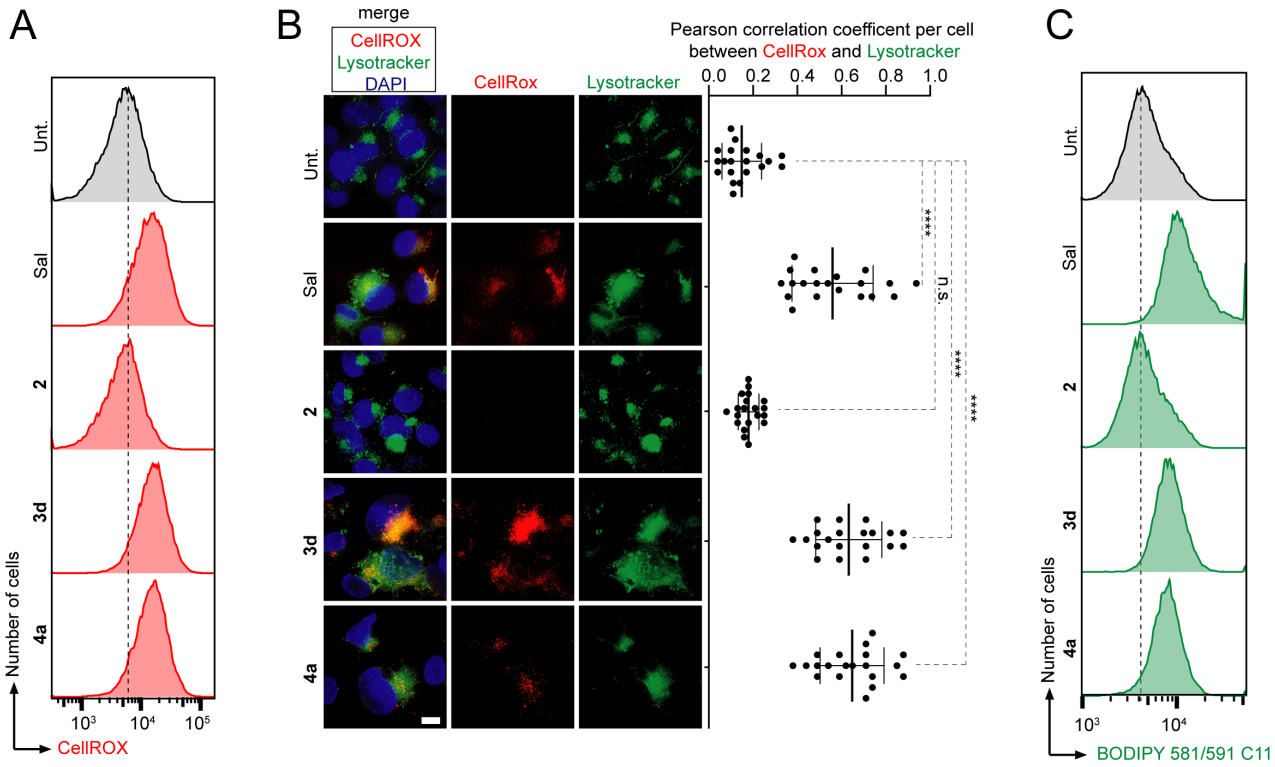

Figure 2. DMT1 inhibitors 3d and 4a promote the production of lysosomal ROS lipid peroxidation. A) Flow cytometry analysis of fluorescence of CellROX in cells treated with **1**, **2**, **3d** and **4a** for 48 h. **B)** Fluorescence microscopy analysis of CellROX fluorescence and Lysotracker. Cells were treated with **1**, **2**, **3d** and **4a** for 48 h. CellROX fluoresces upon ROS induction (red), lysotracker stains the lysosomes (green) and DAPI stains nuclear DNA (blue). Scale bar, 10 µm. Quantification of 20 cells per condition. Colocalization analyses expressed as Pearson correlation coefficients. N = 3 biological replicates. Kruskal-Wallis test with Dunn's correction. Bars and error bars, mean values +/- SD. * $P \leq 0.05$, ** $P \leq 0.01$, *** $P \leq 0.001$, **** $P \leq 0.0001$. **C)** Flow cytometry analysis of lipid ROS in cells treated with **1**, **2**, **3d** and **4a** for 48 h using BODIPY 581/591 C11. HMLER $CD44^{high}/CD24^{low}$ cells were used throughout the figure.

We next investigated the capacity of **3d** and **4a** to kill CSC using physiologically relevant models. To this end, we chose a) primary breast cancer cells, b) the triple-negative human breast cancer cell line MDA-MB-468 and c) primary lung circulating tumor cells (CTC) that recapitulate properties of disseminating cells susceptible to promote metastatic spread. We promoted epithelial-to-mesenchymal transition (EMT)[1, 15] leading to mesenchymal $CD44^{high}$ cell populations using cytokines, epithelial growth factor (EGF) or transforming growth factor ß (TGF-ß). Induction of EMT was further confirmed by western blotting monitoring CD44 and the mesenchymal proteins vimentin and fibronectin (Figure S4). We next assessed the IC_{50} values of cell viability for **1**, **3d** and **4a** in these cells in the epithelial ($CD44^{low}$) and stem-like mesenchymal ($CD44^{high}$) states.

10.1002/chem.202000159

	1	**3d**	**4a**
IC_{50} primary breast $CD44^{low}$ in µM	21.6	4.0	26.1
IC_{50} primary breast $CD44^{high}$ in µM	5.1	1.3	5.9
Ratio primary breast $CD44^{low}/CD44^{high}$	**4.2**	**3.1**	**4.4**
IC_{50} MDA-MB-468 $CD44^{low}$ in µM	6.5	2.4	4.6
IC_{50} MDA-MB-468 $CD44^{high}$ in µM	2.7	0.6	1.1
Ratio MDA-MB-468 $CD44^{low}/CD44^{high}$	**2.4**	**4.0**	**4.2**
IC_{50} lung CTC $CD44^{low}$ in µM	29.3	8.0	44.3
IC_{50} lung CTC $CD44^{high}$ in µM	11.1	1.4	8.8
Ratio lung CTC $CD44^{low}/CD44^{high}$	**2.6**	**5.7**	**5.0**

Table 2. IC_{50} values of cell viability measured for primary breast cancer cells, MDA-MB-468 cells and lung CTC treated with **1**, **3d** and **4a** for 72 h. Selectivity ratios ($CD44^{low}/CD44^{high}$) are indicated, with values >1 indicating a selectivity for cells with CSC properties.

We found that **4a** exhibited a selectivity for primary breast cancer cells in the mesenchymal state comparable to that found for **1** and that both **3d** and **4a** showed significant selectivity for $CD44^{high}$ MDA-MB-468 cells and $CD44^{high}$ lung CTC in the range of 4.0-5.7 fold, which was superior to the selectivity observed for **1**, ranging between 2.4-2.6 fold (Table 2, Figure S5). Taken together, these data indicate that DMT1 inhibitors can selectively kill cancer cells with stem-like properties by interfering with lysosomal iron regulation.

Here, we have generated a library of small molecule inhibitors of DMT1 function and evaluated their capacity to specifically target cells with CSC properties. Some of these molecules, notably **3d** and **4a**, show an efficiency and selectivity for these cells in the same order of magnitude or better than **1**, which remains a benchmark molecule in the context of CSC targeting. We found that, like **1**, these molecules promote increased iron loading in lysosomes, leading to ROS production, lysosomal membrane permeabilization and cell death reminiscent of ferroptosis. The MoA of these molecules may involve other complex components given that DMT1 can also be found in the outer mitochondrial membrane and at the plasma membrane [16]. Since mitochondrial metabolism is upregulated in certain subsets of CSC[3c] and since mitochondrial iron and copper homeostasis play a central role in the maintenance of these cells[17], inhibition of DMT1 activity may impact on mitochondrial iron metabolism, which could potentially be exploited for therapeutic benefits. This study establishes DMT1 function as a tractable strategy to specifically target the CSC niche. This

provides a basis for the development of innovative anti-cancer treatment modalities to avoid cancer relapse and metastasis formation, which constitutes an unmet health need for cancer patients.

Acknowledgements

We thank the CNRS, INSERM and Institut Curie for generous funding. R.R. laboratory is supported by the European Research Council (grant agreement No [647973]), the Fondation Charles Defforey-Institut de France and Ligue Contre le Cancer (Equipe Labellisée). Région Ile de France is gratefully acknowledged for financial support of the 500 MHz NMR. A. V. is funded by PSL Research University and A.L.T. by Fundació Pedro i Pons and Spanish Ministerio de Educacion, Cultura y Deporte. We acknowledge the PICT-IBiSA@Pasteur Imaging Facility of Institut Curie, member of the France-BioImaging national research infrastructure. We thank P. Le Bacon for assistance with high-resolution microscopy. We thank A. Puisieux for providing us with HMLER cell lines.

References

[1] a) M. A. Nieto, R. Y. Huang, R. A. Jackson, J. P. Thiery, *Cell* **2016**, *166*, 21-45; b) T. Brabletz, R. Kalluri, M. A. Nieto, R. A. Weinberg, *Nat Rev Cancer* **2018**, *18*, 128-134; c) I. Pastushenko, A. Brisebarre, A. Sifrim, M. Fioramonti, T. Revenco, S. Boumahdi, A. Van Keymeulen, D. Brown, V. Moers, S. Lemaire, S. De Clercq, E. Minguijon, C. Balsat, Y. Sokolow, C. Dubois, F. De Cock, S. Scozzaro, F. Sopena, A. Lanas, N. D'Haene, I. Salmon, J. C. Marine, T. Voet, P. A. Sotiropoulou, C. Blanpain, *Nature* **2018**, *556*, 463-468.

[2] a) D. C. Voon, R. Y. Huang, R. A. Jackson, J. P. Thiery, *Mol. Oncol.* **2017**, *11*, 878-891; b) S. Müller, T. Cañeque, V. Acevedo, R. Rodriguez, *Isr. J. Chem.* **2017**, *57*, 239-250.

[3] a) T. T. Mai, A. Hamai, A. Hienzsch, T. Cañeque, S. Müller, J. Wicinski, O. Cabaud, C. Leroy, A. David, V. Acevedo, A. Ryo, C. Ginestier, D. Birnbaum, E. Charafe-Jauffret, P. Codogno, M. Mehrpour, R. Rodriguez, *Nat.Chem.* **2017**, *9*, 1025-1033; b) D. Basuli, L. Tesfay, Z. Deng, B. Paul, Y. Yamamoto, G. Ning, W. Xian, F. McKeon, M. Lynch, C. P. Crum, P. Hegde, M. Brewer, X. Wang, L. D. Miller, N. Dyment, F. M. Torti, S. V. Torti, *Oncogene* **2017**, *36*, 4089-4099; c) S. Müller, F. Sindikubwabo, T. Cañeaue, A. Lafon, A. Versini, B. Lombard, D. Loew, T.-D. Wu, C. Genestier, E. Charafe-Jauffret, A. Durand, C. Vallot, S. Baulande, S. Servant, R. Rodriguez, *BioRxvie* **2019**, doi.org/10.1101/693424; d) A. Hamai, T. Cañeque, S. Müller, T. T. Mai, A. Hienzsch, C. Ginestier, E. Charafe-Jauffret, P. Codogno, M. Mehrpour, R. Rodriguez, *Autophagy* **2017**, *13*, 1465-1466.

[4] P. B. Gupta, T. T. Onder, G. Jiang, K. Tao, C. Kuperwasser, R. A. Weinberg, E. S. Lander, *Cell* **2009**, *138*, 645-659.

[5] H. Waldmann, L. Laraia, G. Garivet, D. J. Foley, N. Kaiser, S. Müller, S. Zinken, T. Pinkert, J. Wilke, D. Corkery, A. Pahl, S. Sievers, P. Janning, C. Arenz, Y. Wu, R. Rodriguez, *Angew. Chem. Int. Ed.* **2019**.

[6] M. Tabuchi, T. Yoshimori, K. Yamaguchi, T. Yoshida, F. Kishi, *J. Biol. Chem.* **2000**, *275*, 22220-22228.

[7] a) H. A. Wetli, P. D. Buckett, M. Wessling-Resnick, *Chem. Biol.* **2006**, *13*, 965-972; b) L. Xie, W. Zheng, N. Xin, J. W. Xie, T. Wang, Z. Y. Wang, *Neurochem. Int.* **2012**, *61*, 334-340.

[8] J.-J. Cadieux, Z. Zhang, M. Mattice, A. Brownlie-Cutts, J. Fu, L. G. Ratkay, R. Kwan, J. Thompson, J. Sanghara, J. Zhong, Y. P. Goldberg, *Bioorg. Med. Chem. Lett.* **2012**, *22*, 90-95.

[9] Z. Zhang, V. Kodumuru, S. Sviridov, S. Liu, M. Chafeev, S. Chowdhury, N. Chakka, J. Sun, S. J. Gauthier, M. Mattice, L. G. Ratkay, R. Kwan, J. Thompson, A. B. Cutts, J. Fu, R. Kamboj, Y. P. Goldberg, J. A. Cadieux, *Bioorg. Med. Chem. Lett.* **2012**, *22*, 5108-5113.

[10] a) A. P. Morel, M. Lievre, C. Thomas, G. Hinkal, S. Ansieau, A. Puisieux, *PLoS One* **2008**, *3*, e2888; b) B. Elenbaas, L. Spirio, F. Koerner, M. D. Fleming, D. B. Zimonjic, J. L. Donaher, N. C. Popescu, W. C. Hahn, R. A. Weinberg, *Genes Dev.* **2001**, *15*, 50-65.

[11] M. Niwa, T. Hirayama, K. Okuda, H. Nagasawa, *Org. Biomol. Chem.* **2014**, *12*, 6590-6597.

[12] S. J. Dixon, K. M. Lemberg, M. R. Lamprecht, R. Skouta, E. M. Zaitsev, C. E. Gleason, D. N. Patel, A. J. Bauer, A. M. Cantley, W. S. Yang, B. Morrison, 3rd, B. R. Stockwell, *Cell* **2012**, *149*, 1060-1072.

[13] T. Hirayama, K. Okuda, H. Nagasawa, *Chem. Sci.* **2013**, *4*, 1250-1256.

[14] M. Conrad, D. A. Pratt, *Nat. Chem. Biol.* **2019**, *15*, 1137-1147.

[15] I. Pastushenko, C. Blanpain, *Trends Cell Biol.* **2019**, *29*, 212-226.

[16] N. A. Wolff, A. J. Ghio, L. M. Garrick, M. D. Garrick, L. Zhao, R. A. Fenton, F. Thevenod, *FASEB J.* **2014**, *28*, 2134-2145.

[17] a) K. Laws, G. Bineva-Todd, A. Eskandari, C. Lu, N. O'Reilly, K. Suntharalingam, *Angew. Chem. Int. Ed.* **2018**, *57*, 287-291; b) S. Müller, A. Versini, F. Sindikubwabo, G. Belthier, S. Niyomchon, J. Pannequin, L. Grimaud, T. Cañeque, R. Rodriguez, *PLoS One* **2018**, *13*, e0206764.